Transversal Thermal Conductivity of HTS Tapes: Analytical Method vs Measurements

P. Lammintaus, M. Lyly, D. Sotnikov, and T. Salmi

(Invited Paper)

Abstract—**Design of ReBCO HTS magnets requires reliable data about the tape and insulation thermal conductivities. Material properties represent one of the largest uncertainties when simulating the HTS magnet thermal behavior during magnet cooling, operation, and possible quench scenarios. In this study, we aimed to measure transversal thermal conductivity of insulated and non-insulated HTS tape stacks. Measurements were done in the vacuum of a conduction cooled cryostat. This allows near adiabatic boundary conditions. The measurement results were compared with an analytical model based on thermal conductivities from literature sources. It is noteworthy that the uncertainties associated with the tape material layer thicknesses already constitute a major uncertainty in the magnet analysis. Furthermore, we discuss the challenges, lessons learned and possible future improvements in the measurement methodology.**

Index Terms—**ReBCO HTS tapes, thermal conductivity measurement.**

I. Introduction

DESIGN of ReBCO High-Temperature Superconductor (HTS) magnets requires modeling the heat diffusion processes in the magnet during its cooling, operation, and possible quench events [1], [2]. These simulations rely on the input data about the thermal conductivities and specific heats of the different materials, and in some cases also the thermal contact resistances of the material interfaces. The lack of reliable data about the material properties typically represents one of the largest uncertainties in simulations. It is possible to find data about material properties at cryogenic temperatures from literature, but often measurements are made on "bulk" materials (copper, Hastelloy, silver, YBCO), which may not necessarily correspond to the ones in the ReBCO tape that are manufactured with different thin layer deposition techniques. Moreover, it is not easy to determine accurately the exact geometry of all involved materials such as the thickness of each material layer in the tape, let alone the interface conditions between tapes, cables, or external components. Therefore, an understanding of the reliability of the literature values and different methods to compute effective thermal conductivity is needed, alongside with measurements of real tapes in representative conditions.

In the study presented in this paper, we continued our previous effort to develop accurate ad-hoc measurement methodologies for small-scale experiments relevant to HTS magnet design and analysis at Tampere University, Finland.

We aimed to measure the transversal thermal conductivity of insulated and non-insulated HTS tape stacks and compare the measurement results with an analytical model based on literature material properties. The measurements were done in the vacuum of a conduction cooled cryostat. This allows near adiabatic boundary conditions and simplifies the measurement set-up. The uncertainty analysis for the analytical model considers the thickness variation ranges of the tape material layers, as specified by the manufacturer. The purpose of this work is to determine experimentally a model for quick and realistic heat spreading computation in the solenoid we are going to produce.

The method for measurement of longitudinal thermal conductivity of HTS tape is well described in [30]. Previous works by others related to HTS tape transversal direction thermal conductivity measurements can be found in [3], [4], [11]. In the study by N. Bagrets, et al., thermal conductivity measurement results for SuperPower YBCO tape are presented. The measurements are done in longitudinal and transversal directions of the tape and in a wide range of temperatures. The transversal direction measurements are for soldered tape stacks. In the study by M. Bonura, et al., REBCO coated conductors (CCs) from various manufacturers are measured for transversal thermal conductivity. They found that the measured thermal conductivity varied strongly between the tapes from different manufacturers. Partially this can be explained by different substrate and copper thicknesses. In the study by H. Bai, et al., thermal conductivity measurements for SuperPower YBCO tape stack are presented. In between YBCO tapes there were stainless steel tapes. The sample holder in the study was very similar to the one we constructed.

In Section II we describe the preparation of the tape stacks and then in Section III the design and realization of the sample

Manuscript received 26 September 2023; revised 20 December 2023; accepted 23 January 2024. Date of publication 5 February 2024; date of current version 20 February 2024. This work was supported in part by Business Finland Co-Innovation Project SMARAGDI, under Grant 3972/31/2019 and in part by the Academy of Finland Project Super20T, under Grant 324887. *(Corresponding author: P. Lammintaus.)*

P. Lammintaus and T. Salmi are with Tampere University, 33720 Tampere, Finland (e-mail: patrik.lammintaus@tuni.fi).

M. Lyly was with Tampere University, 33720 Tampere, Finland. He is now with Quanscient, 33100 Tampere, Finland.

D. Sotnikov was with Tampere University, 33720 Tampere, Finland. He is now with Paul Scherrer Institute, 5232 Villigen, Switzerland.

Color versions of one or more figures in this article are available at https://doi.org/10.1109/TASC.2024.3361884.

Digital Object Identifier 10.1109/TASC.2024.3361884

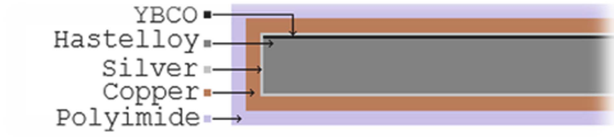

Fig. 1. Insulated tape cross-section geometry. Non-insulated tape cross-section is the same but without the polyimide layer.

TABLE I
SuperOx HTS Tape Material Thicknesses

Material	Thickness
YBCO	2 µm
Hastelloy	63 ± 3 µm
Silver	2 ± 0.5 µm
Copper	20 ± 4 µm
Polyimide (only in insulated tape)	20 ± 4 µm

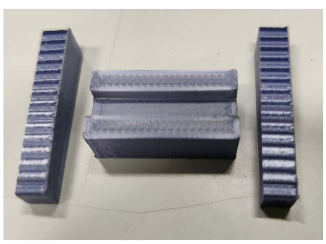

Fig. 2. 3D-printed mold.

holder and measurement set-up. In Section IV we describe the used analytical model for effective thermal conductivity calculation. In Section V we report the measurement results and their comparison with the analytical model. The findings and lessons learned are discussed and concluded in the Section VI.

II. Tape-Stack Samples

The considered tape stacks consist of ten SuperOx HTS tapes [5] glued on top of each other. Each tape includes Hastelloy layer as a substrate, the buffer layer, about 2 µm thick YBCO layer, and the protective silver and copper layers all around the tape [6], [7]. The insulated and non-insulated tapes are otherwise similar, but the insulated one has a polyimide insulation around it [5], [7], [8]. The cross-section of the insulated tape is shown in Fig. 1. Table I summarizes the layer thicknesses and manufacturing tolerances provided by the producer. The glue used between tapes was Stycast 2850FT epoxy [9], [10].

A 3D-printed PLA mold and stair-tools were used to assist in the accurate assembly of the stacks, see Fig. 2. A 24-mm-long piece of HTS tape was inserted into the groove of the mold. Then a layer of glue was spread on top of the HTS tape piece. Then, the next piece of HTS tape was placed on top of the glue layer. After placing the tenth HTS tape piece, the stack was pressed together with a weight of 0.75 kg. The aim was to let the epoxy glue between the tapes overflow out and end up with a HTS tape stack where all glue layers have similar thickness. The bottom and the top surfaces of the stack were covered with masking tape to prevent the glue from spreading there. After the epoxy dried, the stack was trimmed from the excess overflown glue. A photo of the construction phase of the HTS tape stack is shown in Fig. 3, and the final stacks in Fig. 4. The physical dimensions of the samples were measured with a caliper and are shown in Table II. One tape piece in the middle of the stack was left longer. The longer tape piece allowed a temperature sensor placement in the middle of the stack.

Fig. 3. Photo during the stack construction.

Fig. 4. HTS tape stacks. The top stack contains non-insulated tapes. The bottom stack contains insulated tapes.

TABLE II
HTS Tape Stack Physical Dimensions

	Insulated stack	Non-insulated stack
Length (mm)	24.2 ± 0.6	23.5 ± 1.5
Width (mm)	4.50 ± 0.05	4.60 ± 0.05
Thickness (mm)	1.80 ± 0.05	1.35 ± 0.05

This assembly with Stycast-glued tapes corresponds to a small, impregnated solenoid currently under study at TAU. Transversal thermal conductivity of our tape stack samples is expected to be much lower compared to stacks built without stycast, for example in [3], [4].

III. Measurement Setup in Conduction-Cooled Cryostat

The sample holder was designed to measure two identical tape stack samples at the same time, as in [11]. However, in this work it was used only for one sample due to limitations in the electronics related to the temperature sensor readings. In the measurement the other sample location was filled with an insulating block.

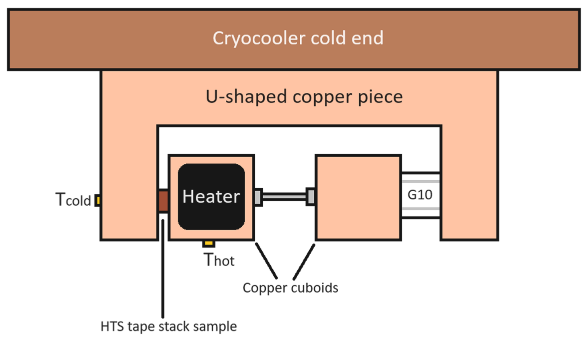

Fig. 5. Thermal conductivity measurement setup principle. The sample holder was designed to measure two identical samples simultaneously. In this work only one sample was measured, and the other was replaced by an insulating block (G10).

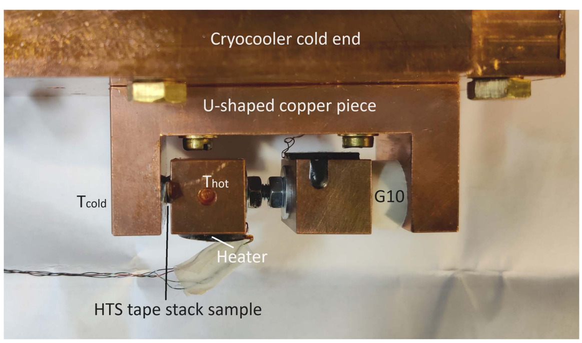

Fig. 6. Measurement setup.

A. Sample Holder

The principle of the sample holder is to allow placing the tape stack between two copper volumes, and to control the temperature of the copper blocks with heaters and the GM type cryocooler, Cryomech GB04. Temperature sensors are placed in the copper pieces and to stack to allow the measurement of temperature gradients. A schematic diagram of the system is shown in Fig. 5. A photo of the system in Fig. 6.

The sample holder consists of a u-shaped copper piece, two small copper cuboids, stainless steel bolt and nuts, a short G10 tube (to replace the missing HTS sample), and a copper radiation shield. The u-shaped copper piece is in direct contact with the cold end of the cryocooler. The copper cuboids and a bolt and nuts are in the middle of the sample holder. A sample and the G10 tube are compressed against the u-shaped copper piece by tightening the nuts. Two surfaces of the sample are now in contact with two copper mediums.

The copper pieces were prepared by machining a 25 mm thick Luvata OFE-OK copper block [12]. The radiation shield was made from 4 mm thick cryocopper sheet. The RRR value of the copper in the radiation shield is about 150, and the OFE-OK copper parts have a guaranteed RRR-value of over 400. The high RRR-value of the copper causes it to have a high thermal conductivity at cryogenic temperature. This allows the copper parts to remain more uniformly at a certain temperature.

The sample holder consists of copper, stainless steel and G10 pieces. All these materials have similar thermal expansion properties. When the sample holder is cooled down, all the different materials are expected to shrink at shared rate, so the sample holder setting will not tighten or loosen. [13]

The purpose of the G10 tube is to insulate the other end of the sample holder. The goal is that all heat from the heater flows towards the sample. Since the G10 tube doesn't have perfect thermal resistivity, it will leak some of the produced heat. The aim was to minimize this heat leakage.

The sample holder is covered with a radiation shield. The radiation shield is in contact with the cold end of the cryocooler. The radiation shield removes most of the radiation heat transfer. The built sample holder radiation shield couldn't completely cover the sample holder. The remaining gaps were covered with reflective tape.

Thermal conductivity between contacts was improved with Apiezon N grease [14]. For example, the contact between the radiation shield and the cold end, and the contact between the sample holder and the cold end. The grease was also used for the contacts of the sample and copper pieces. However, the purpose is different. By applying a layer of grease to the contact of two surfaces, the thermal resistance of the contact can be approximated by using literature. If the contact is under mild pressure, the thermal resistance of the contact can be estimated from [15]. Estimation of the contact resistances helps in understanding the thermal conductivity measurement results. The temperature difference measured across the sample will be caused by the tape stack and additionally by the contact resistances. If the thermal conductivity of the tape stack is calculated based on the whole temperature difference, the resulting thermal conductivity value will be too low by default. The effect of contact resistances is removed during measurement analysis.

If the sample holder was used for two tape stacks, as it was originally intended, then the G10 tube would be replaced with another identical tape stack. Both copper cuboids would have a heater element to produce equal amount of heat flow towards both tape stacks. Then the temperature difference between the two stacks would be measured and analyzed. One benefit for this kind of setup would be the absence of leakage route for produced heat. Now the only possible leakage route would be the instrumentation wires. However, there are also risks in this kind of setup. Building two identical tape stacks could prove to be difficult. If the tape stacks thermal resistances are significantly different, then the heat flow through each stack could be hard to determine, and the thermal conductivity could not be calculated.

B. Temperature Sensors

Four temperature sensors were placed to the measurement setup. Fig. 7. illustrates the sensor locations. Sensors A and B are the most important for the analysis. Sensor A was placed to the copper piece that was connected to the cryocooler 2nd stage, and it measures the colder temperature, T_{cold}. Sensor B was placed to the copper cuboid on the other side of the sample, and it measures the higher temperature, T_{hot}. The copper pieces have a very high thermal conductivity, so their temperature is assumed to be constant. The temperature difference between the sensors A and B will express approximately the temperature

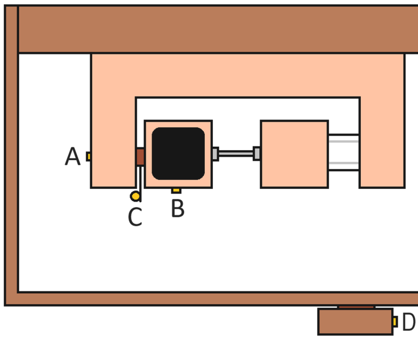

Fig. 7. Temperature sensor locations.

difference between the two ends of the sample. Sensor C was placed on the middle (the 5th) tape of the tape stack, which was left longer for this purpose. The temperature measurement of sensor C can be used to examine the thermal conductivity for half of the tape stack.

Sensor D was placed to the point where the heater wires were anchored. The point D was selected from the bottom of the sample holder's radiation shield. A single 390 Ω resistor was attached to control the temperature of this point. The temperature of the heater wire anchor point is important to keep close to the temperature of sensor B point. Lower temperature difference between these points will result in a lower leakage heat flow through the heater wires. Temperature sensor wiring has the same problem, but the issue is much less significant. Therefore, all temperature sensor wiring was just anchored to the second stage of the cryocooler without any further modifications.

The temperature sensors were attached to the measurement points in two different ways. Sensor A, B, and D were attached to appropriately sized holes. Sensor C was placed inside a copper cylinder. The copper cylinder was soldered to the desired measurement point. Regardless of the method of attachment, Apiezon N grease was applied to the contacts of the temperature sensor and measurement point.

All temperature sensors are Cernox cryogenic temperature sensors by Lake Shore Cryotronics Inc [16]. The sensors are type CX-1070, with calibration data ranging from 4.00 K to 325 K. Using the calibration data, temperature of the sensor can be obtained by measuring the resistance of the sensor. Certain resistance of the sensor corresponds to a certain temperature. We used three high precision multimeters (2 of HP3458A and 1 of HP34420A) to measure the resistances of three Cernox temperature sensors [17], [18].

C. The Heater Element

The heater element consists of two 390 Ω resistors in series, varnish insulation coating, stycast glue coating, and a four-wire configuration to supply current and measure voltage over the resistors. The heater is attached to the point B copper cuboid with stycast coating (see Fig. 5). Two resistors were used to make the heat flow more uniform towards the sample holder.

The heater element wires generally have higher risk for leakage heat in comparison to the temperature sensor wires. When heat energy has an option to flow through temperature sensor wires, there are always significantly more thermally conductive route options available. In comparison, when heat is produced in the heater element, the heat conduction routes available are through the heater element stycast medium towards the rest of the sample holder or through the heater wires. In this case the heater wire conduction route is not negligible. To minimize the heat flow through the heater wires, the length of the wires should be maximized, the thickness of the wires minimized, and the heater wires should be anchored to a temperature as close as possible to the heater temperature.

A DC current source HP6181C was used for supplying power for the heater element [19]. The supplied power was measured using a Fluke 45 dual display multimeter for current measurement and a handheld Fluke 177 True-RMS multimeter for voltage measurement [20], [21].

D. Measurement Procedure

Measurements were performed as follows:

1) 2nd stage temperature T_{cold} is kept constant (e.g., 15 K), and desired power Q_{heater} is applied.
2) System is stabilized to the required temperature range of 0.001 K,
3) Data for temperature difference $T_{\mathrm{cold}}–T_{\mathrm{hot}}$ and heater power Q_{heater} are collected.

Steps 1–3 were repeated for different Q_{heater} values. Then, measurements were repeated for several temperatures of T_{cold}.

E. Reducing the Environmental Heat Load From the Measurement Data and Solving the Stack Thermal Conductivity

Environmental heat load causes temperature difference ΔT_{env} across stack while heater power $Q_{heater} = 0$ mW. Initial temperature difference is subtracted from the measured temperature difference ΔT_{tot}. Then the temperature difference due to heater induced heat flow is $\Delta T_{heater} = \Delta T_{tot} - \Delta T_{env} = T_{hot} - T_{cold} - \Delta T_{env}$

The stack thermal conductivity, *k*, is solved from:

$$k = \frac{d \times Q_{\mathrm{heater}}}{A \times \Delta T_{\mathrm{heater}}} \tag{1}$$

Where Q_{heater} is the heater power through the stack, d and A are the thickness and the area of the stack, ΔT_{heater} is the temperature difference of copper volumes caused by Q_{heater}. The analysis for solving the thermal conductivity is based on the approach presented in [22]. In (Eq. 1), ΔT_{heater} consists of heater-made temperature difference of the stack and the contact resistances. Because of this, the resulted stack thermal conductivity will be too low by default. To exclude the contact resistance component from the result, $\Delta T_{contact}$ is subtracted from ΔT_{heater} in the analysis phase. The determination of $\Delta T_{contact}$ is described in section V. B.

F. Analytical Model for Stack Thermal Conductivity

Effective transversal thermal conductivity of HTS tape stacks is calculated analytically based on the expected geometry and

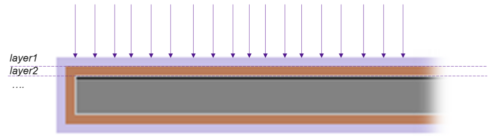

Fig. 8. Cross-section of SuperOx HTS tape. The analytical effective thermal conductivity was determined by first solving the effective thermal conductivities of the different layers, then for the whole tape.

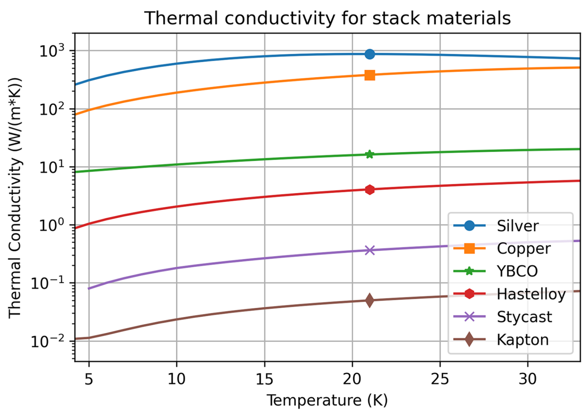

Fig. 9. Thermal conductivity for stack materials in different temperatures [23], [24], [25], [26], [27], [28]. Copper RRR is 12 based on our previous measurements that is very close to value in [29]. The purity of the silver in the tape is not known. However, the effect of a thin layer of silver on the overall thermal conductivity is insignificant. A silver RRR of 30 was used in analytical model.

material properties extracted from literature sources [23], [24], [25], [26], [27], [28]. Effective thermal conductivity of each different horizontal layer is first calculated with (Eq. 2). For the different horizontal layers, the material across the thickness is constant, but may have different materials in parallel (e.g., insulation, copper, and silver). The concept of different layers is highlighted in Fig. 8.

$$k_{eff}^{\text{parallel}} = \sum_{i}^{n} k_i f_i \tag{2}$$

Then, the effective thermal conductivity of whole tape is calculated assuming the different horizontal layers are in series:

$$k_{eff}^{\text{series}} = \frac{1}{\sum_i^n \frac{f_i}{k_i}} \tag{3}$$

Where k_i is effective thermal conductivity of layer i, and f_i is the percentage of the layer i thickness compared to stack thickness. The individual material properties obtained from the literature [23], [24], [25], [26], [27], [28] are shown in Fig 9.

IV. Measurement Results and Comparison With Analytical Model

A. Measurement Results

Table III summarizes the applied heater powers (Q_{heater}), the measured temperature differences across the stack ($T_{\text{cold}} - T_{\text{hot}}$) and the computed thermal conductivities (k). The esimated effect of contact resistances has been removed when computing the thermal conductivity k.

TABLE III
Measurement Results

Insulated stack			Non-insulated stack		
Q_{heater} (mW)	T_{hot} (K)	k $\left(\frac{W}{m*K}\right)$	Q_{heater} (mW)	T_{hot} (K)	k $\left(\frac{W}{m*K}\right)$
T_{cold} = 15 K					
0	15.5908		0	15.1406	
5.633	15.8404	0.4188	5.650	15.2611	0.7301
12.51	16.1283	0.4336	12.55	15.4247	0.6944
22.01	16.5488	0.4269	22.06	15.6478	0.6861
T_{cold} = 17.5 K					
0	18.0203		0	17.6130	
5.585	18.2425	0.4608	5.600	17.7266	0.7970
12.43	18.5251	0.4532	12.46	17.8655	0.7941
21.89	18.9098	0.4538	21.95	18.0546	0.7996
T_{cold} = 20 K					
0	20.4905		0	20.0881	
5.540	20.7009	0.4821	5.553	20.1956	0.8201
12.35	20.9548	0.4896	12.38	20.3281	0.8161
21.79	21.3203	0.4831	21.84	20.5094	0.8203
T_{cold} = 22.5 K					
0	23.0944		0	22.5634	
5.500	23.2938	0.5095	5.513	22.6523	0.9449
12.27	23.5382	0.5096	12.30	22.7706	0.9270
21.68	23.8724	0.5131	21.73	22.9453	0.8894
T_{cold} = 25 K					
0	25.4348		0	25.0735	
5.465	25.6157	0.5418	5.475	25.1628	0.9736
12.21	25.8378	0.5515	12.23	25.2722	0.9783
21.58	26.1703	0.5352	21.63	25.4257	0.9750

The measurement set-up described here gave reproducible results, when the same stack was measured twice. The thermal conductivity of the non-insulated stack was measured a second time. The second time measurements were performed at temperatures ∼15 K, ∼20 K, and ∼25 K. The new thermal conductivity results were within ±14% of the corresponding results in Table III. The average difference between the new k result and the k result of Table III was 6%.

The sensor C measured the temperature in the middle of the stack T_{middle} all the time. Thermal conductivity of half of the stack computed using sensor A and C ($T_{\text{cold}} - T_{\text{middle}}$) was consistently 10–15% lower than the thermal conductivity computed with sensors A and B ($T_{\text{cold}} - T_{\text{hot}}$). The sensors A–B measure the thermal conductivity of 10 tapes and 9 stycast layers. The sensors A–C measure the thermal conductivity of 5 tapes and 5 stycast layers. The percentage of stycast in between the measurement A–C is greater which explains the lower thermal conductivity.

B. Uncertainties in the Measurement

There were several sources of error in the measurements. Not all of the heater power passes through the sample because the insulating piece at the opposite end of the sample holder leaks some of the heat produced. The heat leakage was estimated for both sample measurements. In the case of the insulated tape stack, the heat leakage is less than 5%. For the non-insulated tape stack, the heat leakage is less than 1%. There may also be heat leakage into or out of the heater element through the heater wires. The heater element wiring is anchored to a slightly higher temperature than the heater element temperature.

The uncertainty of multimeters and power sources can be ignored because of their high accuracy. The uncertainty of CERNOX sensor calibration data is ± 9 mK (Calibrated in 2023). However, additional error may occur due to poor sensor mounting. There is vacuum of $5e^{-5}$ mbar inside the cryostat. The convection component of the measurement setup can be ignored.

The total error of thermal conductivity is calculated by "propagation of uncertainty". The calculation of k was presented earlier in (Eq. 1). The uncertainty δk is calculated using (Eq. 4).

$$\delta k = \sqrt{\sum_{i=1}^{6} \left(\frac{\partial k}{\partial x_i} \cdot \delta x_i \right)^2} \quad (4)$$

x_i is measurements V, I, d, l, w, and ΔT. δx_i is measurement uncertainties δV, δI, δd, δl, δw, and $\delta(\Delta T)$. Please note the different symbols δ and ∂ denote the uncertainty and the differential derivative, respectively. Also, the heat power Q_{heater} from (Eq. 1) is divided into voltage and current, V and I, and the area A is divided into length and width, l and w. The main factor contributing to the uncertainty in k is the uncertainty of the temperature difference measurements.

Apiezon N grease was applied to the stack to sample holder contacts. The grease contact causes a temperature difference proportional to heat flow Q_{tot} across the contact [15]. Q_{tot} of a measurement is derived using (Eq. 5).

$$Q_{tot} = Q_{env} + Q_{\text{heater}} = \frac{\sum_i^n \frac{Q_{\text{heater,i}} \Delta T_{env}}{\Delta T_{\text{heater,i}}}}{n} + Q_{\text{heater}} \quad (5)$$

Where $Q_{heater,i}$ is heater power, $\Delta T_{heater,i}$ is the temperature difference caused by the heater. i represents different heater power used at each temperature point T_{cold}. n = 3 for 3 heater powers used at each temperature point T_{cold}.

The contact conductance for the stack to copper grease contact G_{contact} can be determined from fit provided in [15]. The contact resistance is then solved with (Eq. 6).

$$\Delta T_{\text{contact}} = \frac{Q_{tot}}{G_{\text{contact}}} \quad (6)$$

The stack measurement has two grease contact surfaces. $\Delta T_{contact}$ is reduced two times from ΔT_{heater} during the analysis phase. The reduced $\Delta T_{contact}$ varies from 0.01 K to 0.06 K. It is worth noting that the effect of contact resistances has been reduced from the Table III k results. The contact resistance component reduction is done based on literature conductance fit presented in [15].

C. Measurements Vs Analytical Model

Measurement results are presented in Figs. 10 and 11. The horizontal uncertainty of the datapoints represent the temperature range in the measurement. Vertical error bars show the estimated measurement uncertainties based on (Eq. 4). Upper and lower limits of analytical thermal conductivities are based on the tape geometry uncertainties (Table I).

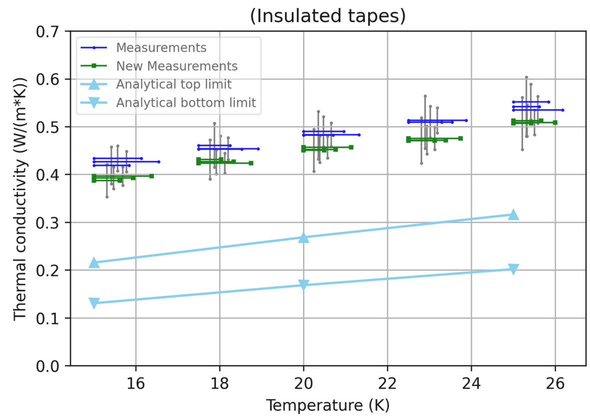

Fig. 10. Insulated tape stack thermal conductivity. The upper and lower limits of the analytical estimation are based on the upper and lower limits given to the tape geometry.

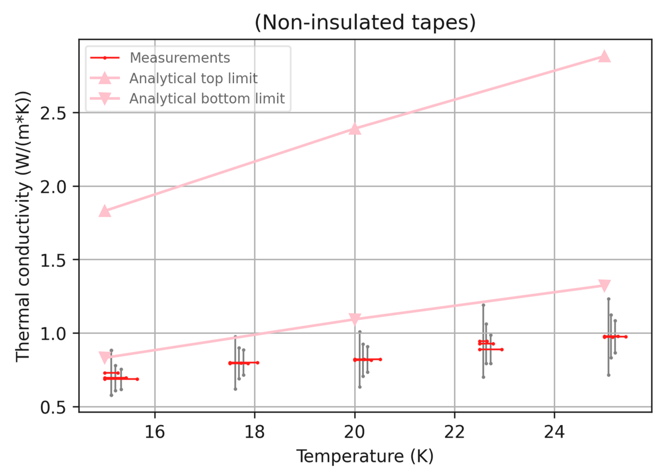

Fig. 11. Non-insulated tape stack thermal conductivity. The upper and lower limits of the analytical estimation are based on the upper and lower limits given to the tape geometry.

"Measurements" were computed based on data from Table III. "New Measurements" refers to measurements done with same stack sample, but after the set-up was improved. The other unused copper cuboid in the sample holder was replaced with G10 tube to let the applied heater power leak less and go more fully through the stack sample. However, if the non-insulated tape stack would be measured again with the improved set-up, the change from the original results would be much smaller, because of its higher thermal conductivity.

The analytical model underestimates the thermal conductivity in the case of insulated stack and overestimates it in the non-insulated stack.

V. Discussion

The measurement set-up seemed to produce repeatable measurement data in the conditions that it was used. However, the measured thermal conductivities significantly deviated from the expectation based on analytical model: up to +165% for insulated and up to −45% for non-insulated stack. If all material properties were correct, and measurement set-up appropriate, one could expect the measurement to give slightly lower k due to the presence of thermal resistances at the material interfaces.

In the case of insulated stack however the measured thermal conductivity is significantly better than the computed one. One possible reason could be the that the used literature value for polyimide thermal conductivity does not correspond to the material in the conductor.

Regarding the reliability of the measurement, the designed sample holder was not used in its optimal configuration, because it was used for only one sample instead of two. However, the error related to this was estimated to be less than 5%. Also, the estimated reading uncertainties in the measurement cannot explain such large "error" in the measurement. Further investigation of the experimental uncertainties could include SEM measurement of the tape stack cross-section and its dimensions, further analysis of the contact resistances, and measurement of different lengths of tape stack as well as more careful alignment of tapes in the stack to reduce the error related to the tape stack area. Also, the number of the temperature sensors within the tape stacks could be increased and the number of tapes could be varied, to get more statistics to the measurement data. Also, the sample holder could be used for two identical samples simultaneously, or the insulation block replacing the other material could be improved.

However, when considering real magnet design, it is important to notice that also the analytical model suggests that the tape stack transversal thermal conductivity can vary up to 100% based on the manufacturing uncertainties about tape layer thicknesses. The material property fits from literature have their uncertainties ($10-15\%$), but in reality, the uncertainty is much larger, because the measurements have been done for differently manufactured materials than in the tape.

VI. Conclusion

The difference between measured and analytical computations calls still for more analysis regarding the measurement set-up accuracy and possible adjustments in the analytical model assumptions. This result highlights the importance of adding a sufficient safety margin in the thermal analysis during the magnet design. Using the thermal conductivities from literature and the nominal tape geometries may lead to large errors in the estimated thermal conductivities. Moreover, in case accurate analysis is needed, it would be useful to be able to characterize the material properties of the individual tape layers and compare with the measurement data from bulk materials.

References

[1] T. Salmi et al., "A novel computer code for modeling quench protection heaters in high-field Nb_3Sn accelerator magnets," *IEEE Trans. Appl. Supercond.*, vol. 24, no. 4, Aug. 2014, Art. no. 4701810.

[2] E. Harö et al., "Quench considerations and protection scheme of a high field HTS dipole insert coil," *IEEE Trans. Appl. Supercond.*, vol. 23, no. 3, Jun. 2013, Art. no. 4600104.

[3] N. Bagrets, W. Goldacker, A. Jung, and K.-P. Weiss, "Thermal properties of ReBCO copper stabilized superconducting tapes," *IEEE Trans. Appl. Supercond.*, vol. 23, no. 3, Jun. 2013, Art. no. 6600303.

[4] M. Bonura and C. Senatore, "Transverse thermal conductivity of REBCO coated conductors," *IEEE Trans. Appl. Supercond.*, vol. 25, no. 3, Jun. 2015, Art. no. 6601304.

[5] A. Molodyk et al., "Development and large volume production of extremely high current density YBa_2Cu_3O7 superconducting wires for fusion," *Sci. Rep.*, vol. 11, no. 1, 2021, Art. no. 2084.

[6] J. Zhu, S. Chen, and Z. Jin, "Progress on second-generation high-temperature superconductor tape targeting resistive fault current limiter application," *Electron. (Basel)*, vol. 11, no. 3, 2022, Art. no. 297.

[7] A. Molodyk and D. C. Larbalestier, "The prospects of high-temperature superconductors," *Science*, vol. 380, pp. 1220–1222, 2023.

[8] J. ter Harmsel et al., "Magnetization loss and transport current loss in ReBCO racetrack coils carrying stationary current in time-varying magnetic field at 4.2 K," *Supercond. Sci. Technol.*, vol. 36, no. 1, 2023, Art. no. 015011.

[9] C. Barth et al., "Degradation free epoxy impregnation of REBCO coils and cables," *Supercond. Sci. Technol.*, vol. 26, no. 5, 2013, Art. no. 055007.

[10] M. Pekarčíková et al., "Analysis of thermo-physical properties of materials suitable for thermal stabilization of superconducting tapes for high-voltage superconducting fault current limiters," *J. Thermal Anal. Calorimetry*, vol. 138, no. 6, pp. 4375–4383, 2019.

[11] H. Bai, W. D. Markiewicz, J. Lu, and H. W. Weijers, "Thermal conductivity test of YBCO coated conductor tape stacks interleaved with insulated stainless steel tapes," *IEEE Trans. Appl. Supercond.*, vol. 23, no. 3, Jun. 2013, Art. no. 4600204.

[12] OFE Copper Products, Luvata Oy. Accessed: Jan. 28, 2024. [Online]. Available: https://www.luvata.com/products/ofe-copper-products

[13] J. Ekin, *Experimental Techniques for Low-Temperature Measurements: Cryostat Design, Material Properties and Superconductor Critical-Current Testing*. Oxford Univ. Press, 2006, pp. 234–235. [Online]. Available: https://doi.org/10.1093/acprof:oso/9780198570547.001.0001

[14] A. N. Grease, M&I Materials Ltd. Accessed: Jan. 28, 2024. [Online]. Available: https://apiezon.com/products/vacuum-greases/apiezon-n-grease/

[15] J. Ekin, *Experimental Techniques for Low-Temperature Measurements: Cryostat Design, Material Properties and Superconductor Critical-Current Testing*. Oxford Univ. Press, 2006, pp. 63, 66–67. [Online]. Available: https://doi.org/10.1093/acprof:oso/9780198570547.001.0001

[16] Cernox product overview, 2016. Accessed: Jan. 28, 2024. [Online]. Available: https://www.lakeshore.com/products/categories/overview/temperature-products/cryogenic-temperature-sensors/cernox

[17] 3458A Digital Multimeter, 8.5 Digit, 2024. Accessed: Jan. 28, 2024. [Online]. Available: https://www.keysight.com/us/en/product/3458A/digital-multimeter-8-5-digit.html

[18] 34420A Nano-Volt/Micro-Ohm Meter, 7.5 Digit, 2024. Accessed: Jan. 28, 2024. [Online]. Available: https://www.keysight.com/us/en/product/34420A/micro-ohm-meter.html

[19] 6181C Current Source, 2024. Accessed: Jan. 28, 2024. [Online]. Available: https://www.keysight.com/us/en/product/6181C/current-source.html#

[20] 45 dual display multimeter, Accessed: Jan. 28, 2024. [Online]. Available: http://www.smart-inc.com.tw/uploads/root/fluke45.pdf

[21] Fluke 177 True-RMS Digital Multimeter, 2024. Accessed: Jan. 28, 2024. [Online]. Available: https://www.fluke.com/en-us/product/electrical-testing/digital-multimeters/fluke-177

[22] I. Hiltunen, A. Korpela, H. Laine, J. Lehtonen, M. Lyly, and R. Mikkonen, "Measured performance of different solders in Bi2223/Ag current leads," *IEEE Trans. Appl. Supercond.*, vol. 18, no. 2, pp. 1427–1430, Jun. 2008.

[23] C. Y. Ho et al., "Thermal conductivity of the elements: A comprehensive review," 1974, (silver).

[24] Material Properties: OFHC Copper (UNS C10100/C10200). NIST, Accessed: Jan. 28, 2024. [Online]. Available: https://trc.nist.gov/cryogenics/materials/OFHC%20Copper/OFHC_Copper_rev1.htm

[25] J. Feng, "Thermohydraulic-quenching simulation for superconducting magnets made of YBCO HTS tape," 2010, p. 18: a-axis preannealing, range 0-200 K.

[26] J. Lu, "Physical properties of Hastelloy® C-276TM at cryogenic temperatures," *J. Appl. Phys.*, vol. 103, no. 6, pp. 064908–064908–6, 2008. [Online]. Available: https://doi.org/10.1063/1.2899058

[27] S. Nakamura et al., "Specific heat, thermal conductivity, and magnetic susceptibility of cyanate ester resins–An alternative to commonly used epoxy resins," *Cryogenics (Guildford)*, (Stycast2850FT, range 2-300 K, p. 79), vol. 95, pp. 76–81, 2018. [Online]. Available: https://doi.org/10.1016/j.cryogenics.2018.09.001

[28] NIST, "Material properties: Polyimide (Kapton)," Accessed: Jan. 28, 2024. [Online]. Available: https://trc.nist.gov/cryogenics/materials/Polyimide%20Kapton/PolyimideKapton_rev.htm

[29] M. Bonura et al., "High-field thermal transports properties of REBCO coated conductors," *Supercond. Sci. Technol.*, vol. 28, 2014, Art. no. 025001.

[30] N. Bagrets et al., "Thermal properties of 2G coated conductor cable materials," *Cryogenics*, vol. 61, pp. 8–14, 2014.